

Encoding The Fine-Structured Mechanism of Action Potential Dynamics with Qualitative Motifs

Robert Clewley†

This preprint is currently under review. Please do not distribute.

Abstract This work presents a neuroinformatic method for deriving mechanistic descriptions of fine-structured neural activity. This is a new development in the computer-assisted analysis of dynamics in conductance-based models, which is illustrated using single compartment models of an action potential. A sequence of abstract, qualitative motifs is inferred from this analysis, forming a template that is independent of the specific equations from which they were abstracted. The template encodes the assumptions behind the model reduction steps used to derive the motifs, and so specifies quantitative information about their domains of validity. The template representation of a mechanism is converted to a hybrid dynamical system, which is simulated as a sequence of low-dimensional reduced models (in this example, phase plane models) with appropriate switching conditions taken from the motifs. We demonstrate the validity of the template on a detailed single neuron model of spiking taken from the literature, and show that the corresponding hybrid system simulation closely mimics the spiking dynamics of the full model.

Keywords Computer-assisted modeling · Model reduction · Qualitative inference · Neuroinformatics · Hybrid dynamical systems · Asymptotic analysis · Multiscale dynamics

PACS 87.10.Ed · 87.19.1l · 87.18.-h

Mathematics Subject Classification (2000) 37D99 · 37M05 · 37M99 · 65L11 · 68W25 · 92-08

Supported by NSF CISE/CCF-0829742 and a Georgia State University Brains & Behavior Seed Grant.

†Neuroscience Institute and Department of Mathematics and Statistics
Georgia State University, Atlanta, GA 30303
Tel.: +1-404-413-6420
E-mail: rclewley@gsu.edu

1 Introduction

The applied sciences currently lack an informatic framework to manage the understanding and development of dynamical models for complex, adaptive behaviors. The necessary combination of insight from data and model analysis requires computer-assisted strategies as data and hypotheses become ever more detailed. Existing strategies are typically based in machine learning and automata theory, and are still in their infancy (Bradley et al, 2001; Coiera, 1992; Fishwick et al, 1994; de Jong and van Raalte, 1999; Reynolds et al, 2002; Zhao, 1994, and references therein). This paper suggests part of a neuroinformatic framework in the context of detailed neural models. For illustrative purposes we apply our analysis to action potential (AP) genesis in single compartment neural models. This is classically described by the space-clamped Hodgkin-Huxley (HH) differential equations (Hodgkin and Huxley, 1952). For a sufficiently large applied current parameter, solutions to these four ODEs exhibit an AP due to the interplay between sodium and potassium ionic currents (Na/K). Specifically, we aim to:

- Examine the detailed dynamic structure behind action potential generation involving fast sodium and delayed rectifier potassium currents.
- Represent this structure according to formal criteria, which are conserved across models that use different versions of the spiking currents as well as additional modulatory currents.
- Provide an explicit definition of a hybrid dynamical system to simulate the resulting reduction.

Our approach relies on dominant scales reduction (Clewley et al, 2005), a technique that assesses the changing roles of variables governed by a dynamical system of ordinary differential equations (ODEs) or differential-algebraic equations (DAEs). The technique decomposes a high dimensional

system into several lower dimensional models and associated algebraic constraints. The constraints provide an explicit domain of validity for the reduced models with appropriate initial conditions because they quantify the underlying assumptions of the reduction. The computer implementation of the dominant scales algorithms permits more rapid hypothesis development and testing of mechanistic descriptions for systems exhibiting multiple scales, and in practice achieves the results of singular perturbation analysis (Eckhaus, 1979; Jones, 1994) without the need for paper and pen. For instance, in previous work we reduced ODEs for biophysical models of AP generation to sub-systems equivalent to those found by singular perturbation analysis (Clewley et al, 2005). Although this was an encouraging validation of the reduction technique, there were three shortcomings that are addressed in this paper:

- The derivation of reduced regimes was based on rough heuristics and was not algorithmic.
- There was no direct determination of a hybrid dynamical system from the abstract regime descriptions, in order to test the qualitative correctness of the regime descriptions by direct simulation.
- Neither the previous version of the dominant scale analysis nor the singular perturbation analysis explicitly determine the time courses of all variables during the AP. In particular, the correct motion of quasi-static slow variables was not explicit in the derived slow manifold equation (Suckley and Biktashev, 2003). The success of the AP mechanism is sensitive to the precise motion of these variables in tandem (see Section 4.1).

The new approach in this paper allows an approximate but explicit description of the slow variables’ motion. This is achieved through the addition of new dominant scale quantities that are monitored during the analysis. We introduce a goal that ensures a rational basis for deriving reduced regimes: to find one common regime description across AP model exemplars. This goal is an objective criterion for regime derivation through a form of optimization, even though we are not yet in a position to automate the derivation. Although we focus specifically on the part of the dynamics involved with the AP and the regeneration of excitability, our approach could be generalized to other common features of the dynamics in order to establish objective criteria for their representation.

In this work we derive the template description from analysis of periodic solutions of the model equations, but the success of our approach does not depend on periodicity. In fact, our approach is inherently apt to analyze transient dynamics. The decomposition to piecewise-low-dimensional models differs from traditional a priori reductions of the 4-dimensional HH model to 2D models such as those of Fitzhugh (1961) or Morris and LeCar (1981). Our approach

makes no prior assumptions about the salient characteristics to retain or about the presence of small parameters in the model, which instead are determined adaptively and algorithmically. However, we sacrifice the convenience of a single (i.e., globally applicable) low-dimensional description, and use a hybrid dynamical systems formalism resembling the piecewise asymptotic reductions of multiple time scale systems.

We quantify some heuristic aspects of phase plane views during the AP and gain an intuitive appreciation for what the asymptotically-derived formal regimes mean geometrically and mechanistically. As a result of these refinements to the dominant scale method we show that the Na/K AP mechanism can be understood as a sequence of two-dimensional dynamical systems, and furthermore that it can be abstracted to a sequence of logical rules for the salient dynamical changes in the ion channels. We then demonstrate that the set of decomposed sub-systems from our analysis constitute a sufficiently self-contained “template” description of the AP dynamics by coding the regimes and the transitions between them into a hybrid dynamical system model. Simulation of that model qualitatively reproduces the desired behavior.

Decomposing complex systems into template descriptions is a practical basis for concisely representing, understanding, and designing dynamic mechanisms in biology. If the template is appropriately abstracted from the detailed dynamics, it can be a general-purpose description for similar dynamical systems exhibiting similar behavior. The power of the template is assessed by testing it on other models, fine tuning it if necessary to capture only the most fundamental aspects of the mechanism across different instances of a phenomenon.

2 Methods

All computational analysis and simulation was performed using the PyDSTool software environment for dynamical systems (Clewley et al, 2007). PyDSTool is a Python-based, open source package that interfaces legacy ODE and DAE solvers (in C or Fortran) with tools for symbolic mathematics, phase plane analysis, optimization, and model construction. Bifurcation analysis and continuation are also supported via PyCont and its interface to AUTO (Doedel et al, 1991). PyDSTool makes use of the associated Python libraries Numpy (Oliphant, 2006), Scipy (Jones et al, 2001), and Matplotlib (Hunter, 2007). ODEs were solved using the adaptive Dormand-Prince dopri-853 integrator (Hairer et al, 1993). Results were insensitive to moderate changes in integrator parameters, in particular to absolute and relative error tolerances and event detection tolerances. Full code and further documentation for the calculations described here is available at <http://www2.gsu.edu/~matrhc/AP.html>.

2.1 Single compartment model

The membrane potential V of an isolated somatic compartment is governed by a current-balance equation

$$C \frac{dV}{dt} = - \sum I_{\text{ionic}} + I_{\text{applied}}, \quad (1)$$

for a membrane capacitance C , a sum of ionic currents and an applied bias current that is possibly time-varying. Each ionic current takes the form $I_s = g_s s^{p_s} \bar{s}^{q_s} (V - E_s)$ for channel reversal potential E_s , maximum conductance g_s , activation gating variable s and, if present, inactivation gating variable \bar{s} , for some integer powers p and q (possibly 1). Similarly, the applied current is formally denoted $g_a a$ for a maximum current magnitude $g_a = I_{\text{applied}}$ and a formal variable $a \equiv 1$ for the constant applied current used here. The passive leak current is denoted $g_l l (V - E_l)$ with a formal activation $l \equiv 1$. This non-standard notation makes later mathematical definitions uniform at the expense of physiological interpretation of the symbols and uniformity in their units.

The analysis of the action potential (AP) is performed for three different test models, involving only ionic currents for fast sodium (with activation variable m and associated inactivation h), rectifying potassium (with activation variable n and no inactivation variable), and a passive leak. The models exhibit Type I or Type II excitability properties (Rinzel and Ermentrout, 1989). Unless otherwise stated, the ionic gating variables $s = m, h, n$ acting on the somatic compartment are given by

$$\frac{ds}{dt} = (s_{\infty}(V) - s) / \tau_s(V). \quad (2)$$

If a model treats the fast sodium activation as instantaneous then it is instead defined algebraically as $m = m_{\infty}(V)$. The details of the voltage dependent functions and parameter sets for the models are given in Appendix A.

Formally, the *input* variables to the voltage equation are m, h, n, l, a for the models presented here. For notational uniformity in the definitions of dominant scale analysis, conductance-based inputs to the voltage equation belong to the index set $I_1 = \{m, h, n, l\}$ (Clewley et al, 2005). Due to the star-shaped connectivity graph between the dynamic variables (see inset of Fig. 4), we focus analysis on the voltage equation at the hub, which also contains the physiologically measurable membrane potential variable V . The instantaneous time scale of the voltage equation is given by

$$\tau_V = C / \sum_{s \in I_1} g_s s^{p_s} \bar{s}^{q_s}. \quad (3)$$

The asymptotic target voltage is the membrane potential that would eventually be reached if all gating variables were held constant (i.e., the solution to $dV/dt = 0$ at time t for m, h , and n fixed according to their values on the given trajectory

at time t). V_{∞} is available explicitly for the models we consider here and plays the same role as s_{∞} for a dynamic gating variable s :

$$V_{\infty} = \tau_V \left(\sum_{s \in I_1} g_s s^{p_s} \bar{s}^{q_s} E_s + g_a a \right) / C. \quad (4)$$

Eq. (1) can now be rewritten in the same form as Eq. (2):

$$\frac{dV}{dt} = (V_{\infty}(m, n, h) - V) / \tau_V(m, n, h). \quad (5)$$

Loosely speaking, the reciprocal of any instantaneous time scale τ plays the role of a time-varying ‘‘eigenvalue’’ towards a time-varying ‘‘fixed point’’ value (the asymptotic target). If any one the values of $s = m, h, n$ is allowed to vary, the set of values $V_{\infty}(s)$ forms the respective nullcline $\mathbf{N}_s = \mathbf{N}_s(V)$ in the (s, V) phase plane. The V nullcline is denoted $\mathbf{N}_V = \mathbf{N}_V(m, n, h)$. We will introduce a measurement of the phase plane’s autonomy that helps to ensure that the remaining two variables will have minimal effect on this nullcline, so that $\mathbf{N}_V \approx \mathbf{N}_V(s)$ for only one variable s .

2.2 Dominant scale analysis

We now describe each part of the dominant scale analysis, from the concrete quantitative measurements to the qualitative templates. For reference, the relationships between these parts is summarized in Fig. 1.

2.2.1 Influence of inputs on the membrane potential

In a slight deviation to the definitions used previously (Clewley et al, 2005, 2009), the dominance (or influence strength) of an input is measured as a sensitivity, omitting a multiplicative factor of the gating variable. Thus, we define

$$\Psi_s = \left| \frac{\partial V_{\infty}}{\partial s} \right| \quad (6)$$

for each formal input variable $s = m, n, h, l, a$ to Eq. (1). This definition is used because it was found to give greater consistency between the results for all the models analyzed, and to better complement the definition of the rate of influence Ω_s below. The time-varying Ψ_s values are computed along a numerically computed trajectory for the dynamical system. Because of the desired level of detail in our analysis we treat inactivation gating variables separately to their associated activation variables, and both are explicitly represented in the equations. Ψ_s effectively measures the potential effect on V_{∞} of a relative change in the input current I_s to Eq. (1). Given the hub-like connectivity of the dynamic variables, there is no need to measure the influence of V on m, h , or n , which all depend solely on V .

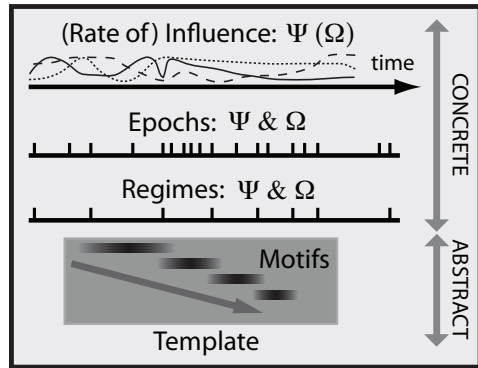


Fig. 1 A schematic summary of the principal concepts used in this paper. Influences Ψ and rates of influence Ω are time-varying measurements from a dynamical systems model along a given trajectory. Epochs are derived from relative changes in Ψ or Ω values. Many superfluous details in epochs can be simplified by aggregating significant changes into a few regimes. The essential changes between regimes are abstracted into changes between logical motifs, which together form a template. Motifs and templates may focus on specific parts of the dynamics associated with a qualitative and functional feature such as an action potential. The concrete concepts are specific to implementations of a model; the abstract concepts are model independent.

The algorithm for determining which inputs are most dominant is detailed in Clewley et al (2005). It uses a scaling threshold σ to compare the relative magnitudes of the Ψ_s at every time point. The most dominant input at time t has the largest $\Psi_s(t)$ value. From this, the active set of inputs at time t is the decreasing-ordered set $\mathcal{A}_\Psi(t)$ of inputs whose Ψ values are all within a factor σ of the largest value. The largest value at time t is denoted $\mathcal{A}_\Psi[1]$. The modulatory set $\mathcal{M}_\Psi(t)$ is determined from the remaining inputs using a second application of the algorithm. This finds the next largest group of inputs, whose Ψ_s are all within a factor of σ of the most dominant inputs remaining. After that, all other remaining inputs are considered inactive.

2.2.2 Time scales of response

Using a threshold γ , the relative time scales τ_s/τ_V of all inputs associated with differential equations are split into fast, order 1 (“normal”) time scale and slow sets, denoted $\mathcal{F}(t)$, $\mathcal{N}(t)$, and $\mathcal{S}(t)$ respectively. A fast variable s has $\tau_s/\tau_V < 1/\gamma$ while a slow s has $\tau_s/\tau_V > \gamma$. When m is defined algebraically it is always in $\mathcal{F}(t)$. In this context, if a variable s is fast or slow its time scale of response to perturbations is fast or slow, regardless of ds/dt .

2.2.3 Instantaneous rate of influence and local autonomy

In addition to comparing the relative sensitivity of a trajectory to all its inputs using Ψ_s we also consider which of the dynamic inputs move quickly enough to make V_∞ change quickly. We define the instantaneous rate of influence

$$\Omega_s = \Psi_s \left| \frac{ds}{dt} \right| = \left| \frac{\partial V_\infty}{\partial s} \frac{ds}{dt} \right| \quad (7)$$

only for the dynamic variables $s = m, h, n$. In models where m is defined algebraically we use the explicit time derivative of $m = m_\infty(V)$ in Eq. (7), obtained from the chain rule. We analyze Ω_s similarly to Ψ_s using the same threshold σ to form corresponding dominant scale sets $\mathcal{A}_\Omega(t)$ and $\mathcal{M}_\Omega(t)$. The Ω_s are more appropriate quantities to compare than the raw velocities ds/dt because we care specifically about the effect of inputs on V . For instance, when $s - s_\infty$ becomes small then ds/dt becomes small. However, the instantaneous effect of s on V_∞ depends on the magnitude of the sensitivity Ψ_s . If Ψ_s is sufficiently large then the effective change to V_∞ remains comparatively large. Although comparing Ψ values determines that the dynamics is potentially influenced by s in a neighborhood of a given trajectory at time t , the Ω values provide a uniform basis for a refined analysis that takes into account more information about the local dynamic inter-dependencies.

Analysis of \mathcal{A}_Ω is crucial to monitoring the autonomy of reduced 2D phase plane representations (s, V) of the AP near a given trajectory segment. When interpreting these graphically it is important to remember that the V equation only “sees” the instantaneous distance $V(t) - V_\infty(t)$ and the s equation only “sees” $s(t) - s_\infty(t)$, regardless of what is happening to the nullclines elsewhere in the picture. While some movement of \mathbf{N}_V is inevitable and necessary, meaningful phase plane views involve minimal movement in a neighborhood of the current value of $V(t)$ as measured by Ω_s . This situation will be referred to as local autonomy. If any nullcline crossings are present in such a neighborhood they correspond to what are known as quasi-static fixed points (qsfp). On the other hand, movement of \mathbf{N}_V far from the current value of $V(t)$ does not affect the local autonomy of the 2D dynamics and may be essential to the progress of a mechanism. Nullcline crossings that are not qsfps are rapidly moving and are referred to here as pseudo fixed points in the phase plane.

We recall some helpful facts about any 2D phase plane projection (s, V) of the higher dimensional dynamics, where $s = m, n$, or h over a given time interval of the AP. The nullcline $\mathbf{N}_s(V)$ is always static in time in the phase plane view because s_∞ is a function of V only. However, \mathbf{N}_V moves as time evolves due to changes in the non-phase plane variables $\hat{s} = m, n$, or h ($s \neq \hat{s}$). The goal is to pick time intervals over which some choice (s, V) provides a sufficiently static \mathbf{N}_V so

that the dynamics are easily interpreted in traditional phase plane terms. We make these choices by monitoring $\Omega_{\hat{s}}/\Omega_s$ along the orbit, switching the phase plane view when any such ratio indicates that \mathbf{N}_V varies too rapidly with respect to any \hat{s} .

2.2.4 Epochs and regimes

Changes in the ordering or constitution of any of the dominant scale sets occur at times referred to as *epoch* changes, and the constitution of the sets between these times defines epochs in the dynamics. Typically, there are many such epochs over the course of a typical trajectory, reflecting detailed changes that may be relatively unimportant. One objective for choosing the scale parameters σ and γ is to minimize the number of epochs the analysis creates, although only values of at least 2 generate non-trivial reductions in these models. In this work we focus on the epochs generated by changes in \mathcal{A}_Ψ and \mathcal{A}_Ω and consider changes in \mathcal{F} and \mathcal{S} to have secondary importance.

As described previously (Clewley et al, 2005), heuristic arguments can be used to aggregate similar or short-lived epochs into a few *regimes*. If well chosen, these regimes can closely resemble the asymptotically-valid descriptions obtained by multiple scale analysis. However, heuristic criteria depend on a user’s subjective requirements for granularity in the analysis, which may change with emerging understanding of the reduced dynamics resulting from trial aggregations. Additionally, there are limitations in any discrete categorization of the nonlinear characteristics of smoothly-varying dominant scale quantities. This means that aggregation possibilities are generally not unique, and thus users must supervise regime derivation.

Tables 2 and 3 in Appendix B show complete ordered sets of \mathcal{A}_Ψ and \mathcal{A}_Ω and their corresponding time intervals for the Type II Hodgkin-Huxley test model, using $\sigma = \gamma = 4$. Those time intervals interleave to give the epoch time intervals shown in Fig. 2. This figure follows the scheme of Fig. 1, graphing the specific dominant scale quantities and the resulting epoch time intervals for this model. The convenience of this logarithmic plot is to compare the normalized scales of the quantities in the same way as the implementation of the epoch-generating algorithm. Thus, all Ψ and Ω influence values are normalized at every time point by the largest of their kind. Epoch changes are caused either when (a) the normalized Ψ values cross the threshold σ (variables enter or leave \mathcal{A}_Ψ), (b) normalized Ω values cross the threshold γ (variables enter or leave \mathcal{A}_Ω), or (c) there are changes in the ordering of these sets. (Note that the excursions to $-\infty$ in these plots are due to the influences being absolute values of derivatives that may pass through zero.)

2.3 Motifs and templates

A *motif* encodes the logic of salient cause-and-effect relationships between variables during one regime. Epochs and regimes are bound to a specific implementation of the dynamics by ODEs and DAEs and explicit intervals of time associated with a given solution to those equations. In contrast, motifs do not depend on a particular implementation of the regime’s dynamics by a specific set of equations and are not tied to explicit intervals of time. Good motifs successfully characterize qualitative features of dynamics in a neighborhood of the trajectory they were derived from. A motif consists of *domain rules* that hold for the duration of the motif’s validity, and *transition rules* for determining when to switch to the next motif. In this simple context motifs are inherently sequential. Transition rules for a motif do not have to remain true for the duration of the next motif unless explicitly controlled by the next motif’s domain rules.

For domain rules the primitive predicates about the dynamics at time t during a motif are described in words as: Input s is most dominant in one of the active input sets \mathcal{A}_Ψ or \mathcal{A}_Ω ; input s belongs to any one of the dominant scale sets; and dynamic input s has a fast, slow, or normal (order 1) time scale. For transition rules these predicates are interpreted as specifying a change, requiring that the predicates must not hold at the beginning of the current motif. Complex predicates can be formed from negations, conjunctions, and disjunctions of the primitive predicates.

A sequence of motifs connected by their transition rules forms a *template*. A template provides an abstract, mechanistic description of the dynamics with a quantifiably verifiable domain of validity in any given implementation of the dynamics.

We study multiple models of AP behavior as a means to optimize a regime derivation that leads to a common template description for all test models. Fig. 2 shows the robust regime aggregations for the Type II HH test model (these aggregations will be derived in the Results). Our template for the Na/K AP will be optimized to hold for three test models. This attempts to ensure that only the salient changes in the dynamics necessary to create an AP will be retained in the description, and provides an objective criterion to aggregate epochs into regimes for the AP feature.

A template can be seen as defining an equivalence class of possible models whose behaviors qualitatively match the template rules, although we do not pursue a formal logic approach to analyzing qualitative dynamics here (Cf. van der Schaft (2004)). At present the optimization is done by hand but it is amenable to automated qualitative reasoning and rule mining techniques (Smolinski et al, 2006).

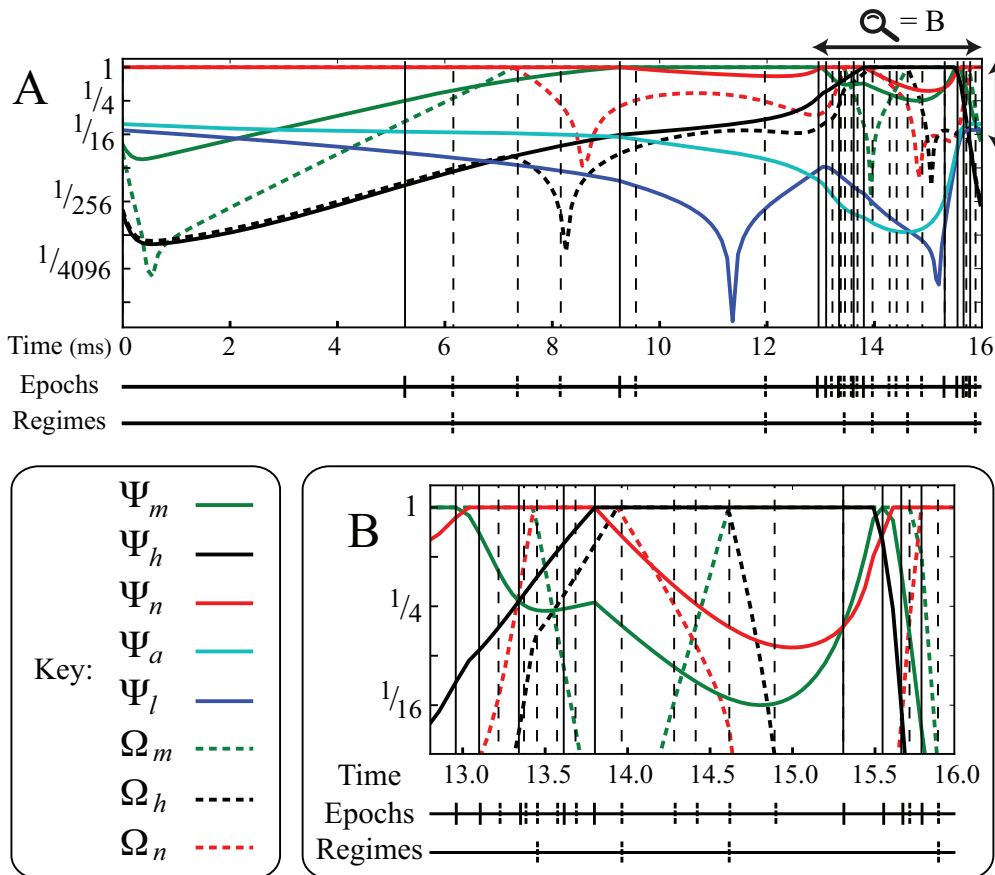


Fig. 2 (A) A graph of all the dominant scale quantities for the Hodgkin-Huxley Type II neuron model. For $\sigma = \gamma = 4$, the epochs for both Ψ (solid vertical lines) and Ω (dashed lines) are shown overlaid. The derivation of regimes as an aggregation of certain epochs is explained in the Results section. (B) The inset region is a magnified part of the action potential.

2.4 Hybrid dynamical system simulation and shadowing

The transitions between motif states resemble a reduction of the AP to symbolic dynamics (Lind and Marcus, 1995). These reduced dynamics can be explicitly simulated as a hybrid system, which is a dynamical system made up of smooth vector fields and state- or time-dependent criteria for switching between them. Our approach to hybrid system simulation is in a similar spirit to other piecewise-reduced model simulations, for instance the “local splitting” of Deuflhard and Heroth (1996) for chemical kinetic equations with multiple time scales. Here, the motif rules directly specify the form of the hybrid simulation of the regime models. This is an improvement over Clewley et al (2009) where transitions between regimes were first simplified by observation of emergent thresholds in variable values that corresponded only loosely to changes in the dominant scale sets. However, checking the motif rules directly requires continual re-

analysis of the dominant-scale sets during the simulation, and would be expensive to perform at every time step. For the sake of efficiency, each regime is simulated for a long time and the resulting trajectory segment is post-processed according to a vectorized dominant scale calculation of all points at once. When the trajectory fails to satisfy the motif rules at a switching time, the next regime is initialized from the trajectory at that time and the simulation continues. The linear sequence of regime simulations halts if the next motif transition rule is never satisfied, at which point an error condition is raised. The initial conditions for the simulation are taken from the unreduced system’s trajectory at the point at which R_I begins.

A theoretical justification of an accurate hybrid systems representation (e.g., van der Schaft and Schumacher (2001)) is not developed here. We present an empirical justification based on comparison of hybrid solutions with solutions to the unreduced model. The extent of the match between

the solutions indicates the extent to which the system naturally separates into low-dimensional approximations. We take advantage of the strongly hyperbolic nature of conductance-based neural dynamics and our control of changing scales through Ψ and Ω . Control is established according to self-consistency arguments that were introduced in Clewley et al (2005) but were not formalized or implemented until now, thus ensuring the “composability” of the hybrid system’s components. In particular, the stronger the separation in dominance between the chosen variables for the regime and those considered modulatory, the better the regime captures that part of the dynamics. Also, rapid changes in the constitution of the dominant scale sets ensure that the transitions between regimes are relatively discrete (i.e., separated by small boundary layers) and therefore well defined as hybrid simulation transition events.

A complicating aspect of the self-consistency arguments is the continued need to represent the dynamics of variables \hat{s} not present in a regime. We may not ignore the dynamics of \hat{s} because the evolution equations are only effectively decoupled in one direction. In the simulation of Eq. (1) \hat{s} values are either held constant from their last value in the previous regime if $\hat{s} \notin \mathcal{F}$, or slaved according to $\hat{s} = \hat{s}_\infty(V)$ if $\hat{s} \in \mathcal{F}$. These reductions reflect the lack of dynamic influence of \hat{s} on V . In the other direction of coupling they are effectively slaved to the changing V , and their V -driven differential equations must be monitored. The monitoring facilitates an ongoing dominant scale analysis of an unreduced version of Eq. (1) in terms of a new variable, V^{shadow} . In particular, this equation involves asymptotic target and time scale terms based on *all* the input variables, i.e. s values from the reduced regime equations and \hat{s} values from the shadowed dynamics. Dominant scale analysis determines when the \hat{s} variables will re-enter the hybrid dynamics in a later regime of the sequence, at which time an updated value of their state to re-initialize the simulation is crucial.

As a simple illustration, consider making a reduced model for the single epoch over $t \in [0, 5.16]$ for the Type II HH model (see Appendix A). This is time interval 1 of Table 2, for which $\mathcal{A}_\Psi = \{n\}$, $\mathcal{M}_\Psi = \{m, a, l\}$. Here, m and h are held constant in the reduced model but are also shadow variables: the evolution of m is tracked so that in the subsequent epoch it joins \mathcal{A}_Ψ and h must be tracked in case the dynamics of the reduced model V cause h to become an active variable. a and l correspond to passive input terms and do not require shadow equations in order to track potential changes in their influence. In this particular epoch, a and l are not in \mathcal{A}_Ψ , and so need not be included in the right hand side of the equation for V at all (formally, we set $a = l = 0$ in Eq. (4)). Although the computational cost of retaining the leak and applied current is minimal, it is physiologically meaningful to consider whether they play a significant role. Thus, we

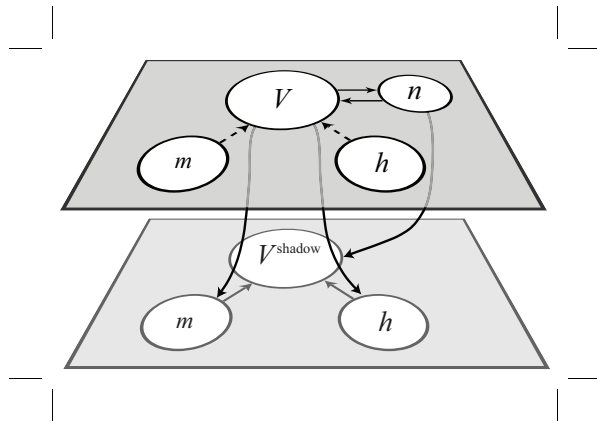


Fig. 3 A schematic representation of shadowing for the first epoch of the Type II Hodgkin-Huxley model’s periodic orbit, in which n is dominant and m and h are held constant in the dynamics of the observed V . The shadow variables m and h evolve according to their original equations except that they are driven by V , and output to the equation for the unreduced ODE Eq. (9) for V^{shadow} . Dominant scale analysis is performed on Eq. (9) to determine when the reduced model ceases to be valid.

can verify, through the hybrid model, that they are not necessary to recreate this part of the unreduced dynamics.

As depicted in Fig. 3, the 2D reduced model for this epoch would be

$$\frac{dV}{dt} = (V_\infty(m_0, n, h_0) - V) / \tau_V(m_0, n, h_0), \quad (8)$$

$$\frac{dn}{dt} = (n_\infty(V) - n) / \tau_n(V),$$

augmented by the shadow system

$$\frac{dV^{\text{shadow}}}{dt} = (V_\infty(m, n, h) - V^{\text{shadow}}) / \tau_V(m, n, h), \quad (9)$$

$$\frac{dm}{dt} = (m_\infty(V) - m) / \tau_m(V),$$

$$\frac{dh}{dt} = (h_\infty(V) - h) / \tau_h(V).$$

for initial conditions $V(0) = V^{\text{shadow}}(0) = V_0$, $m(0) = m_0$, $n(0) = n_0$, $h(0) = h_0$ taken from the known periodic orbit at time 0, the epoch’s start time. Modular model specification tools in PyDSTool allow the symbolic equation structure of the models to be efficiently modified to create the shadowing and reduced version of the equations.

3 Results

Here we develop a template tuned to three variants of the HH equations that exhibit Type I and Type II excitability (Rinzel and Ermentrout, 1989). We study the classic Type II HH parameter regime for the giant squid axon (Hodgkin and Huxley, 1952), a Type I variant of the HH model for an inhibitory cortical interneuron (Kopell et al, 1999), and the

Wang-Buzsáki (WB) interneuron model (Wang and Buzsáki, 1996). For clarity, a phase plane analysis of the possible reduced sub-systems across multiple epochs is discussed in the context of the Type I HH model. The story is similar for the other models. This exploration leads to logical criteria for defining robust regimes from the epochs in all three models, and hence a common template. Finally, the template is successfully tested on a complex model of a tonic spiking neuron that is taken from the literature.

A coarse pattern of changes in influence along the periodic orbits of Hodgkin-Huxley type models is known from previous dominant scale and asymptotic analysis. For instance, in Clewley (2004) and Clewley et al (2005) the AP for the Type I HH neuron was reduced to three 2D regimes using changes in Ψ only. The first regime of those analyses involves the spiking threshold and upstroke behavior dominated by the fast sodium current. The regime captures the pre-spiking “slow passage” effect of being near the ghost of a saddle-node bifurcation (Strogatz, 2001), as discussed below. Here, $m \in \mathcal{F}$, while h and V are the only dynamic active variables. The modulatory dynamics of n act to carry the system to the second coarse regime. This regime encompasses a sequence of interactions between the sodium and potassium variables, and describes the remainder of the upstroke, the peak/plateau and downstroke phases of the AP. These interactions require a pattern of saddle-node bifurcations to occur in the (m, V) phase plane in a timely fashion, driven by quasi-static changes in $n, h \in \mathcal{S}$. This is the only regime that is incomplete as a component of an explicit hybrid system model for the AP, because the motion of n and h is not determined explicitly. The last regime corresponds to the action of the delayed rectifier potassium in the recovery after the AP.

3.1 Deriving AP epochs and regimes

Dominant scale analysis of periodic, tonic spiking trajectories for the three test models was performed using scale separation parameters σ and γ set at several values between 2 and 6. Final values were selected based on two criteria: (1) the ease with which a common template could be derived for all the models, (2) that the template captures enough detail in the slow motion of n and h through an AP that they can be described explicitly in a hybrid model. In general, appropriate σ and γ values may be dependent on the model, a particular parameter set, and choice of initial conditions. The resulting dominant scale sets for the choices $\sigma = \gamma = 4$ are listed in Tables 4-7 of Appendix B.

Our novel use of Ω , the rate of influence measure, will further resolve epoch changes through the second coarse regime, expanding it into three refined regimes of only two dynamic variables each. This is the minimum number of

additional regimes that allow an explicit, self-contained description of the AP dynamics amenable to a hybrid system simulation. Our analysis of an AP will therefore contain a total of five relevant regimes, labeled $R_{\mathbf{I}}-R_{\mathbf{V}}$. We do not further investigate $R_{\mathbf{V}}$ and the subsequent dynamics of the interspike interval because it does not involve a dynamically interesting interplay between currents, and has already been discussed in Clewley et al (2005).

Although our analysis was performed on all three models, we now focus on the specifics of these observations for the Type I HH interneuron model, as it decomposes to phase plane models most cleanly. Figs. 4, 5A and 6 show the phase planes for the upstroke, peak/plateau, and downstroke (respectively) of the AP in the (m, V) view. Each shows consecutively numbered snapshots of the moving nullcline $\mathbf{N}_{\mathbf{V}}(m; n, h)$ in red at equally spaced times over the indicated time intervals. The green curve shows the projection of the periodic orbit to this subspace and time interval. Taken together the trajectory segments in these figures connect to give the entire time course of m and V through the coarse-grained second regime of Clewley (2004), also shown together in Fig. 7. To refine the coarse AP regime, we aggregate epochs until a significant change arises in \mathcal{A}_{Ψ} or \mathcal{A}_{Ω} , and repeat this process until the coarse regime’s changes are completely accounted for.

The primary observations that allow the refinement to three new regimes can be summarized as follows. During an AP peak/plateau, $m \approx m_{\infty}(V)$ so that $dm/dt \approx 0$. Thus, $\Omega_m \approx 0$ and we can temporarily neglect the m dynamics as static while the slow variables n and h each spend some time as the most dominant variables that are moving significantly. Eventually, m leaves the vicinity of $m_{\infty}(V)$ and again becomes the most dominant moving variable.

3.1.1 Building the refined phase plane regimes

According to the definitions in Section 2.4, we seek a sequence of 2D regime models for the AP. Each will consist of equations for V , V^{shadow} , the most active dynamic variable s (according to either Ψ or Ω , as detailed below), and the remaining shadow variables $\hat{s} \neq s$. The phase plane for each model will therefore be (s, V) . The two passive currents (the leak and applied current) are only retained in $R_{\mathbf{I}}$, where they play a role in the depolarization that initiates the AP dynamics.

We begin building $R_{\mathbf{I}}$ at $t = 8.1514$, where we first find that V_{∞} is most sensitive to m ($m = \mathcal{A}_{\Psi}[1]$), and that m moves V_{∞} most dominantly ($m = \mathcal{A}_{\Omega}[1]$). Thus, the appropriate 2D view for $R_{\mathbf{I}}$ is (m, V) , in which there is a single qsfp for large V (Fig. 4). When V depolarizes fully, dm/dt becomes small. At the same time, the growing modulatory effect of $n \in \mathcal{M}_{\Psi}$ on $\mathbf{N}_{\mathbf{V}}$ is occurring far from the $(m(t), V(t))$ values on the trajectory. Indeed, we can observe in Fig. 4 that,

for any of the three instances of $(m(t), V(t))$ shown on the trajectory, the relative motion of $\mathbf{N}_V(t)$ above those points is small. Thus, \mathbf{N}_V remains locally autonomous, as defined in Section 2.2.3. The changes in n cause a saddle-node (SN) bifurcation far from $(m(t), V(t))$, creating pseudo fixed points in the phase plane. (We note for later that this must not occur until V is sufficiently depolarized that it will not get trapped on the hyperpolarized side of the unstable fixed point.) The dominance of m decreases until \mathcal{A}_Ω changes and n most strongly affects \mathbf{N}_V . This corresponds to changing the order of the elements in \mathcal{A}_Ω from $\{m, n\}$ to $\{n, m\}$ (from interval 7 to 8 of \mathcal{A}_Ω in Table 5), and we change regime to R_{II} at $t = 14.0781$. R_{I} incorporates intervals 8–13 of \mathcal{A}_Ψ (Table 4) and 5–7 of \mathcal{A}_Ω . Because intervals 8 and 9 of \mathcal{A}_Ψ include the passive inputs a and l , they are retained in R_{I} .

During the voltage peak of R_{II} we know that n and h move V_∞ until V sufficiently passes the knee of \mathbf{N}_m in the (m, V) view. However, we see in Fig. 5A that $\mathbf{N}_V(m; n, h)$ varies significantly over the time interval $[14.0781, 14.4900]$ in this view. The motion of V_∞ is problematic because it creates a pseudo fixed point near $(m, V) = (1.0, 40)$. Instead, the appropriate 2D view over $[14.0781, 14.3623]$ for R_{II} is (n, V) , where there is a qsfp near $(n, V) = (0.8, -40)$. R_{II} incorporates intervals 13–15 of \mathcal{A}_Ψ and 8–10 of \mathcal{A}_Ω . This continues until h dominates \mathcal{A}_Ω (interval 10 into 11) and we begin R_{III} . The appropriate 2D view over $[14.3623, 14.4900]$ for R_{III} is (h, V) with a qsfp near $(h, V) = (0.1, -40)$. This incorporates intervals 15–16 of \mathcal{A}_Ψ and 11–12 of \mathcal{A}_Ω . Figs. 5B and C show the appropriate phase plane views in which \mathbf{N}_V varies little with respect to the unrepresented variables. The relative autonomy of these views clarifies their interpretation as simple attraction towards a qsfp.

The regime changes to R_{IV} when m moves V_∞ so rapidly that $m = \mathcal{A}_\Omega[1]$. Thus, in R_{IV} the appropriate 2D view is (m, V) , shown in Fig. 6. As required by the mechanism, the effect of n and h on V_∞ is weak near the knee of \mathbf{N}_m , where there is local autonomy. Thus, V_∞ can be trusted not to change rapidly in a way that might prematurely restore the three fixed points through a SN bifurcation and trap V permanently at a depolarized level. As a result, V slowly passes the knee (the ghost of the SN) then rapidly descends towards the hyperpolarized fixed point. The remaining effect of n and h is to bend \mathbf{N}_V at depolarized levels to recreate the pseudo fixed points of R_{II} . This ensures that V fully depolarizes and the system regenerates to an excitable state, and corresponds to the transition to $n = \mathcal{A}_\Psi[1]$. Thus, R_{IV} holds for $t \in [14.4900, 14.8596]$, incorporating intervals 16–20 of \mathcal{A}_Ψ and 13–16 of \mathcal{A}_Ω . The subsequent R_{V} is not analyzed here.

The portion of the original periodic solution of the model equations through the phase plane pictures can be seen in the dotted lines of Fig. 7.

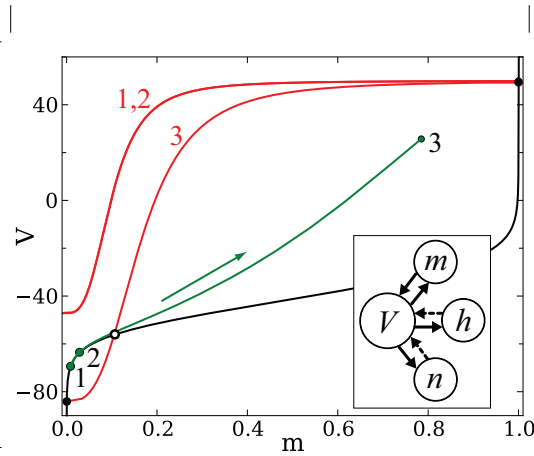


Fig. 4 A sequence of three instances in time during Regime I of the AP during a periodic orbit from the unreduced Type I interneuron model (period 15.1128 ms). The instances are equally spaced in time over $[8.1514, 14.0781]$ (endpoints included). The moving $\mathbf{N}_V(m, h, n)$ is shown in red, the static $\mathbf{N}_m(V)$ in black. The trajectory portion is shown in green with the value of the variables at the time instances shown as green circles. “Fixed points” of the phase plane system are shown by black circles (filled: stable, open: unstable). The inset network diagram shows the effective connectivity of the system during this regime (dashed arrows signify weaker influence).

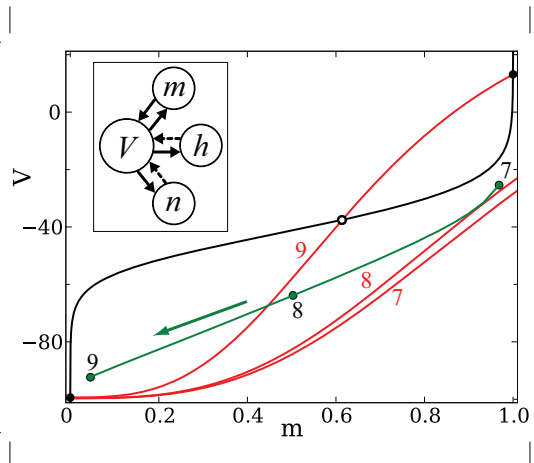


Fig. 6 A sequence of three instances in time during Regime IV of the AP during a periodic orbit from the unreduced Type I interneuron model. The instances are equally spaced in time over $[14.4900, 14.8596]$ (endpoints included).

3.2 Deriving AP motifs and template

The entry condition for the template is that of R_{I} , namely $m = \mathcal{A}_\Psi[1] \wedge m = \mathcal{A}_\Omega[1] \wedge n \in \mathcal{M}_\Omega$. The last term of this conjunction helps to ensure that n will increasingly modulate and eventually become dominant for R_{II} . The choice of predicate rules for the AP template were hypothesized to closely follow the explicit sequence of changes in \mathcal{A}_Ψ and \mathcal{A}_Ω described above for the Type I HH model. However, the exact order of these changes and the exact details of the cri-

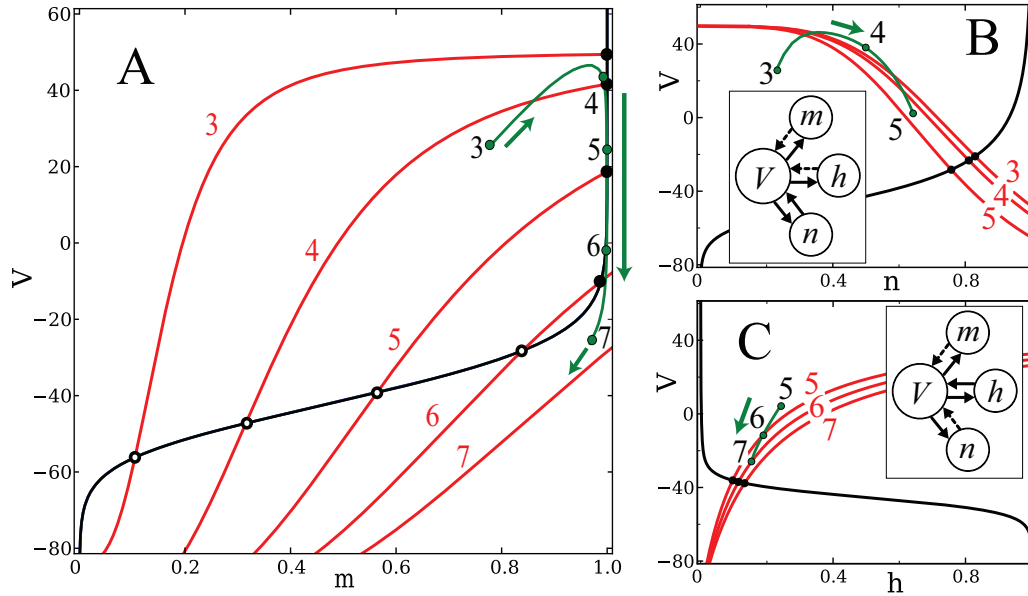


Fig. 5 A sequence of five instances in time during Regimes II and III through the peak of the AP during a periodic orbit from the unreduced Type I interneuron model. The instances are equally spaced in time over $[14.0781, 14.4900]$ (endpoints included). (A) The non-autonomous (m, V) phase plane. (B) The relatively autonomous phase plane (n, V) between instances 1 and 3. (C) The relatively autonomous phase plane (h, V) between instances 3 and 5.

teria were observed to differ between the test models. Many minor adjustments were made to generalize the rules so that they fit all the test models, but here we present two examples:

(1) For the Type I HH model it was observed that m and n remained in \mathcal{A}_Ψ throughout R_{III} . This was hypothesized to be a necessary condition for the downstroke of the AP and encoded as a rule. However, this did not hold in the WB model, where the largest Ψ_m/Ψ_h ratio was approximately $1/10$ during the downstroke. By relaxing the domain rule from $m \in \mathcal{A}_\Psi$ to $m \in \mathcal{A}_\Psi \vee m \in \mathcal{M}_\Psi$, and using a similar relaxation for n , the rule accommodated the difference between models and therefore became more generally applicable.

(2) h was hypothesized as necessarily in \mathcal{S} while it acted as the “quasi-static” bifurcation parameter in the (m, V) phase-plane picture. This assumption did not hold for the WB model, where $\tau_h \sim \tau_V$. Instead, it was sufficient to require that h never joins \mathcal{F} .

Fine-tuning the rules by hand in this way yielded the motif sequence in Table 1. The model APs robustly fit this template when varying σ or γ by up to 25%. In all the test models, regimes $R_{\text{I}}-R_{\text{V}}$ correspond to asymptotic regimes derived in the literature for these or similar models.

3.3 Hybrid dynamical systems simulation

During the above analysis we noted self-consistency conditions that ensure the sequence of changes in \mathcal{A}_Ψ and \mathcal{A}_Ω happen correctly: e.g., that a certain SN bifurcation occurred before the end of a regime. We hypothesize that it is sufficient to monitor the shadow variables and the dominant sets during each phase plane regime model in order to qualitatively reconstruct all the necessary dynamic changes in sequence. According to the hybrid systems definitions taken from the piecewise-reduced regime models described above, all three simulations of the neuron models successfully executed an AP and returned to a recovered state consistent with tonic spiking over a comparable time interval (Fig. 7). All variables \hat{s} not present in the regime had their values held constant in Eq. (1) at their initial values for the regime (indicated by solid squares in the figures).

All transitions between the motif models happened via the transition rules, not by the breaking of domain rules. This is further confirmation of the dynamical similarity between the models and the adequacy of the template. The lack of smoothness in the connection between hybrid trajectory segments is to be expected, and reflects the level of granularity in the analysis and the quality of the regime reductions. Thus, we made no restriction that trajectory segments connect smoothly, which would mainly serve aesthetic pur-

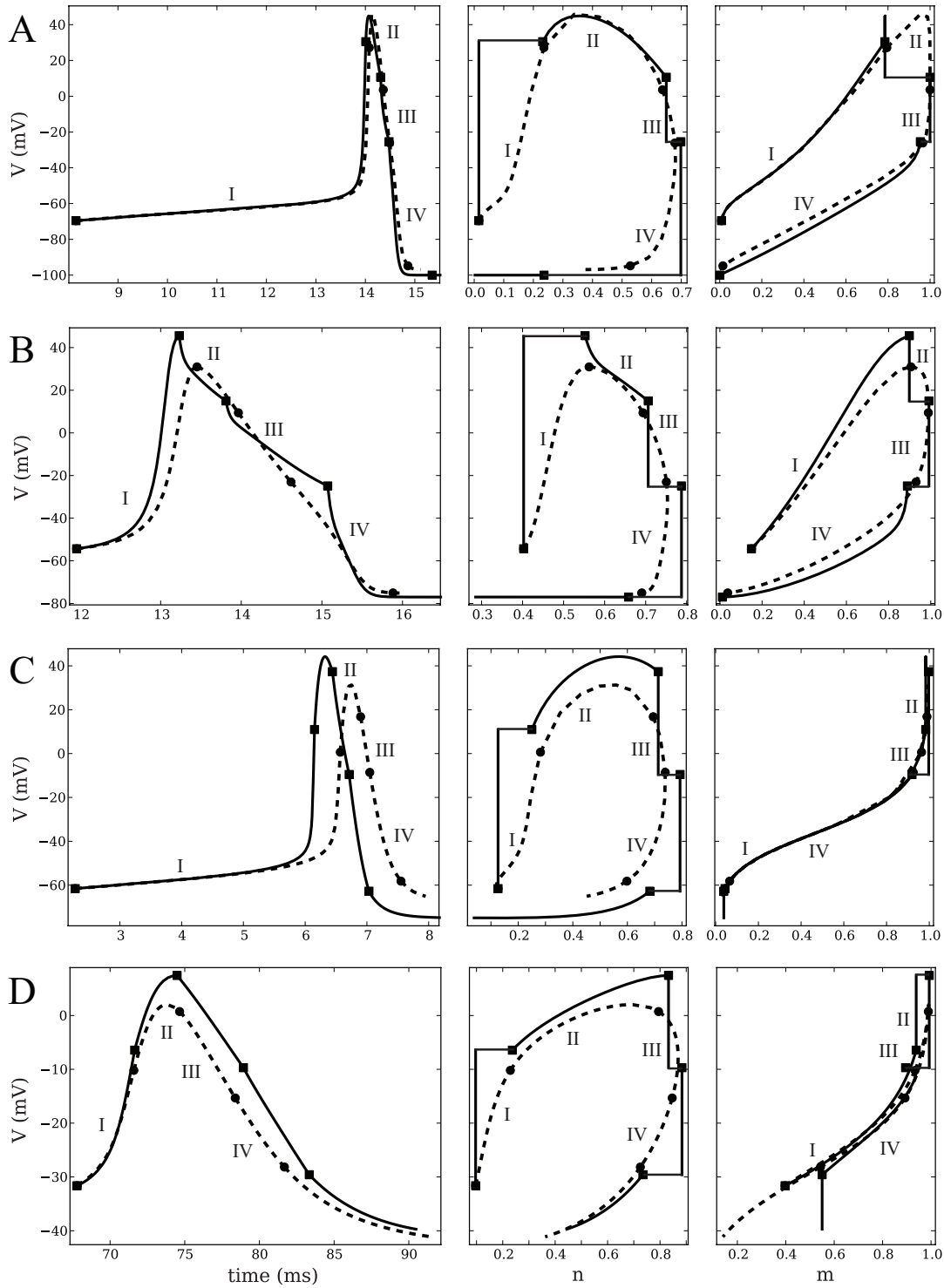


Fig. 7 Comparison of voltage traces and phase plane projections for each unreduced and hybrid model analyzed. The dashed traces show a portion of the periodic trajectory of the unreduced system through Regime IV. Solid traces show the corresponding trajectory of the hybrid system simulation. Markers indicate the start, end or transition between the 4 successive motifs. The left column shows $V(t)$, the middle column shows the (m, V) phase plane, and the right column shows the (n, V) phase plane. Due to some variables being held constant in some regimes, the solid trajectories in the phase plane views are discontinuous curves. (A) Type I interneuron (period 15.1128 ms). (B) Type II Hodgkin-Huxley (period 17.0882 ms). (C) Type I Wang-Buzsáki (period 8.3756 ms). Because m follows an algebraic equation as a function of V in this model, the (m, V) plane does not show an open loop. (D) Type I heart interneuron model (period 141 ms).

Table 1 Domain and transition motif rules making up the AP template, and the appropriate phase planes in which to view the reduced dynamics.

Motif	Phase plane	Domain rule	Transitional rule
I	(m, V)	$m \in \mathcal{A}_\Psi$	$n = \mathcal{A}_\Omega[1] \wedge n \in \mathcal{I}$
II	(n, V)	$n \in \mathcal{A}_\Psi \wedge m \notin \mathcal{A}_\Psi \wedge h \notin \mathcal{F} \wedge n \notin \mathcal{F}$	$h = \mathcal{A}_\Omega[1]$
III	(h, V)	$(m \in \mathcal{A}_\Psi \vee m \in \mathcal{M}_\Psi) \wedge (n \in \mathcal{A}_\Psi \vee n \in \mathcal{M}_\Psi) \wedge h \notin \mathcal{F} \wedge n \notin \mathcal{F}$	$m = \mathcal{A}_\Omega[1]$
IV	(m, V)		$m \notin \mathcal{A}_\Omega$

poses. However, the decomposition of the Type II HH model to a hybrid model of 2D regimes is less distinct than that for the Type I models, making the trajectory segments connect noticeably less smoothly (Fig. 7B). Greater smoothness could be achieved by permitting at least one 3D reduction in the sequence, for instance.

3.4 Testing the template on a complex spiking model

We now test the fit of a more complex model to the AP template, using a 14-variable ODE model for an isolated leech heart interneuron known as HN (Cymbalyuk et al, 2002). This model is a good test due to the complex mixture of currents and the different time scale for AP production (its spiking period is 141 ms compared to 8–15 ms in the previous models). Parameters for its Type I tonic spiking state are given in Appendix A.4. This model contains eight distinct ion channels involving sodium, potassium, and calcium, with kinetics spanning a wide range of time scales. Several of these channels are responsible for the control of bursting activity (existing in a different parameter regime) and as such were not expected to play a role in the tonic spiking AP. From the sequence of epochs derived by dominant scale analysis the conductance of the K1 potassium current was identified as the primary AP recovery variable (the product of the activation and (slow) inactivation variables together playing the role of n). The K2 potassium current also has a minor role in recovery but was hypothesized to be inessential to the basic AP mechanism. As expected, the fast sodium current was identified as responsible for the AP onset (with activation m and inactivation h).

The motif sequence in Table 1 was successfully evaluated along a tonic spiking periodic orbit (Fig. 7D, dotted line) with no changes to the template. However, because of the large number of modulatory inputs not present in the test models, two minor additions to the template were needed in order for its corresponding hybrid system of 2D regimes to successfully simulate an AP: (1) R_I started only when the non-spiking modulatory inputs had either left \mathcal{A}_Ψ (for the persistent sodium current) or had become slow for the duration of the AP (for the K2 potassium current, which remained low in \mathcal{A}_Ψ for the σ and γ used in analyzing the test models). (2) R_{IV} completed when these variables rejoined

\mathcal{A}_Ψ or became normal speed, respectively. The resulting hybrid dynamics (Fig. 7D, solid line) show that the essential pattern of the template holds with only the three primary variables, m , h , and n .

4 Discussion

This work has demonstrated a neuroinformatic technique for inferring and comparing the functional properties of different models of similar phenomena using logical structures (motifs and templates). We used the algorithmic implementation of dominant scales analysis to derive reduced-order models of the dynamics along similar principles to singular perturbation and asymptotic analysis. The abstraction of qualitative motifs from these sub-models encoded well-known insights into the sodium-potassium action potential (Na/K AP). For instance, we observe that the derived R_I – R_{II} correspond to Phases 1–2 (upstroke and then plateau) of Borisjuk and Rinzel (2005); R_{III} and R_{IV} constitute two parts of Phase 3 (downstroke); and R_V corresponds to Phase 4 (recovery). The mechanistic roles of the fast sodium and slow (rectifying) potassium currents were shown to persist in models with different excitability properties and in the context of strong modulatory currents. The use of motifs offers exciting possibilities for improving model analysis and optimization in the context of experimental data and designing novel models for mechanisms. Our approach can also be used to study more complex dynamics in networks and with neurons that exhibit bursts of APs, where intuition is less clear and where parameter tuning by hand is less practicable.

4.1 Comparison to singular perturbation analysis of an AP

Singular perturbation analysis of an excitable system with multiple scales requires that “slow” variables (such as the gating variables n or h) act as bifurcation parameters in the “fast” sub-system reduction of the dynamics (involving V and m) (Jones, 1994; Rubin and Wechselberger, 2007; Suckley and Biktashev, 2003). In this formal analysis, the fast sub-system is a family of phase portraits of (m, V) as the variables (h, n) are slowly varied along the AP trajectory as if they were parameters (hence *quasi-static*). To ensure that the AP evolves correctly, n and h must be precisely varied in

combination to cause the correct pattern of saddle-node bifurcations in the family of phase portraits at the right times with respect to the changing state of V and m , and so properly generate an AP. In contrast, here we demonstrated an explicit determination of the dynamics of n and h during this critical period, albeit at the expense of complete mathematical rigor. The domain of validity conditions and transition rules of motifs provide helpful quantitative information about the degree of perturbation possible from the singular limit and how to switch between asymptotically valid regimes when approximating the low dimensional nature of the dynamics using a hybrid system model.

4.2 Application to integration of levels of analysis in neuroscience

A growing problem in neuroscience is the holistic integration of detailed knowledge about small-scale components with systems-level and behavioral knowledge (for instance, see Villoslada, Steinman, and Baranzini (2009)). A major hurdle in attempting this is the adequacy of natural language descriptions of causal mechanisms at any level of analysis. Such descriptions are crucial in hypothesizing functional roles for ion channels in a somatic compartment, the dendritic structure of a neuron, the connectivity of a whole network, or dynamically changing large-scale network activity. These descriptions involve a sequence of logical conditions about the salient interactions between variables at any given instant.

Unfortunately, mechanistic descriptions involve many assumptions, the technical details of which may not be easily addressed in natural language terms. Although these descriptions can lead to testable hypotheses, this shortcoming can become most problematic when attempting to integrate knowledge at multiple levels, in particular to generate a unified model of a system (Dickinson et al, 2000; Edwards, 2010). The approach espoused in this work is to use algorithmic tools to more reliably define mechanistic hypotheses about biophysical processes described by differential and differential-algebraic equations. Inspired by previous heuristic approaches (such as Ermentrout and Kopell (1998)), as well as established approaches in computer science involving qualitative reasoning and formal verification (Coiera, 1992), we describe causal mechanisms here as a self-consistent logical narrative using reduced regime variables and formalized inter-relationships. More powerful than a static description in natural language, this view is inherently dynamic as it can be embodied in a hybrid dynamical simulation that explicitly validates its underlying assumptions. (This is the same way that any natural language description becomes more explicit when it is simulated as a mathematical model.)

The work of Ermentrout and Kopell (1998) shows an early example of deriving a mechanistic description for the synchronization of a small biophysical neural network. Their analysis suggested a detailed set of logical steps that describe the origins of a stable, synchronized state in terms of the timing and effect of individual APs. In doing so they made several assumptions that are not explicitly verified by either mathematical theory or numerics. Nonetheless, the one-dimensional spike time difference map they derived from these assumptions accurately predicted the rate of synchronization in the system as parameters were varied. This is indirect validation of the assumptions, although the map has no explicitly defined domain of validity. It is therefore unresolved as to how far from synchrony the map applies, which assumptions will fail when initial conditions or parameters are varied far from their original values, or why those assumptions fail.

It must be stressed that a template is only as good as the conditions under which it is expected to perform. As part of an iterative learning process, a template can be modified to accommodate new information about the dynamics further from the “training” trajectory, particularly about how a model can fail to elicit features when parameters are changed or perturbations are made. In future work our approach will be expanded to small network scenarios where the changing time of arrival of AP pulses between neurons during a transient may cause different motif rules to fail and thus produce a transition to different motifs. In that case the paths to different global dynamical outcomes form a network of possible motif states and transitions. An application of this would be to map the valid parameter domain for a global coherent activity state satisfying a certain template by computing the hyper-surface in parameter space on which the template rules fail.

4.3 Application to model optimization and design

A major goal in contemporary computational neuroscience is to achieve more effective model design and optimization based on qualitative specifications. Neural models and data are becoming ever richer. As a result, an approach based on qualitative specifications will improve the fitting of a poorly understood model to experimental data, and aid in the inference of mechanistic motifs that drive qualitative reasoning and computer-assisted synthetic modeling of new models. The optimization algorithms at the heart of such methods may be global or local in nature.

Global optimization methods such as evolutionary algorithms (Achard and De Schutter, 2006) or brute force search (Prinz et al, 2004) are useful for exploring large parameter spaces, especially when fitness function gradients are poorly defined or conditioned. However, global methods may neglect useful information in the local parameter sensitivity of

features that they are seeking and the potentially small size of appropriate parameter regions. For large numbers of free parameters, local gradients can help avoid unnecessary recombinations or mesh refinements to locate small regions of optimal fitness.

A drastic increase in sophistication of model fitness measurement is required to create reliable gradient information that is achievable using desktop computing power. Fitness functions based on qualitative features can reduce the effective dimensionality of the problem by increasing the fidelity and relevance of what they measure. Formally encoding mechanistic descriptions and assumptions using the results of algorithmic dominant scale analysis and bifurcation analysis is one way to facilitate this. Here, we have used dominant scale analysis to encode intuitive and heuristic aspects of the modeling process. In particular, we mined common patterns in activity across different models, and formalized them as measures of similarity that can be used by standard optimization algorithms. These measures can be used to quantify the fit of a model to a template while embedded inside optimization loops. Although the elementary automated reasoning algorithms used here cannot replace human intuition and logic, the level of automation already achieved creates new computational possibilities for computer-assisted modeling. Further coordination with methods from machine learning and optimization theory will develop these possibilities further.

For instance, work in preparation investigates model design by “data-free” optimization. Fitness measures were created in PyDSTool that evaluate the qualitative similarity of a model trajectory to that of a successful AP. These measures used logical and quantitative information from the Na/K AP template (via relative sizes of Ψ and Ω values) and the geometric changes of the reduced phase planes (e.g., the closest distance between nullclines that must eventually cross). As a result, a standard gradient descent optimizer successfully found parameters to fix a broken mechanism that had been induced in the model—no direct comparison to a successful AP voltage trace was necessary. Naturally, this assumes the model is capable of a Na/K AP in principle, but a failure of this optimization process would cast doubt on this hypothesis and provide diagnostic information. An application of this approach would be to design AP dynamics with different sets of currents on a more systematic basis than trial and error. This could include adjusting parameters or functional forms of the gating variable equations to achieve an AP with different varieties of kinetics (e.g., without the use of a sodium inactivation variable). In contrast to related algorithmic approaches by Druckmann et al (2007, 2008); Olypher and Calabrese (2007); Tien and Guckenheimer (2008), dominant scale analysis has the potential to adaptively determine salient features for optimization and reduce human supervision.

Acknowledgements The author would like to thank the anonymous reviewers for their constructive comments and suggestions.

References

- Achard P, De Schutter E (2006) Complex parameter landscape for a complex neuron model. *PLoS Computational Biology* 2(7)
- Borisyuk A, Rinzel J (2005) Understanding neuronal dynamics by geometrical dissection of minimal models. In: Chow C, Gutkin B, Hansel D, Meunier C, Dalibard J (eds) *Models and Methods in Neurophysics*, Elsevier, pp 19–72
- Bradley E, Easley M, Stolle R (2001) Reasoning about nonlinear system identification. *Artificial Intelligence* 133(1):139–188
- Clewley R (2004) Dominant-scale analysis for the automatic reduction of high-dimensional ODE systems. In: Bar-Yam Y (ed) *ICCS 2004 Proceedings*, New England Complex Systems Institute
- Clewley R, Rotstein HG, Kopell N (2005) A computational tool for the reduction of nonlinear ODE systems possessing multiple scales. *Multiscale Modeling and Simulation* 4(3):732–759
- Clewley R, Soto-Treviño C, Nadim F (2009) Dominant ionic mechanisms explored in the transition between spiking and bursting using local low-dimensional reductions of a biophysically realistic model neuron. *J Comput Neurosci* 26(1):75–90
- Clewley RH, Sherwood WE, LaMar MD, Guckenheimer JM (2007) PyDSTool, a software environment for dynamical systems modeling. URL <http://pydstool.sourceforge.net>
- Coiera E (1992) The qualitative representation of physical systems. *The Knowledge Engineering Review* 7(11):55–77
- Cymbalyuk G, Gaudry Q, Masino MA, Calabrese RL (2002) Bursting in leech heart interneurons: cell-autonomous and network-based mechanisms. *J Neuroscience* 22(24):10,580–10,592
- Deuffhard P, Heroth J (1996) Dynamic dimension reduction in ODE models. In: Keil F, Mackens W, Voß H, Werther J (eds) *Scientific Computing in Chemical Engineering*, Springer-Verlag, pp 29–43
- Dickinson MH, Farley CT, Full RJ, Koehl MAR, Kram R, Lehman S (2000) How animals move: An integrative view. *Science* 288
- Doedel E, Keller HB, Kernevez JP (1991) AUTO. *International Journal of Bifurcation and Chaos* 1:493
- Druckmann S, Banitt Y, Gidon A, Schurmann F, Markram H, Segev I (2007) A novel multiple objective optimization framework for constraining conductance-based neuron models a novel multiple objective optimization framework for constraining conductance-based neuron models

- by experimental data. *Frontiers in Neuroscience* 1(1):7–18
- Druckmann S, Berger TK, Hill S, Schurmann F, Segev I (2008) Evaluating automated parameter constraining procedures of neuron models by experimental and surrogate data. *Biological Cybernetics* 99:371–379
- Eckhaus W (1979) *Asymptotic Analysis of Singular Perturbations*. North-Holland, Amsterdam
- Edwards D (2010) Neuromechanical simulation. *Frontiers in Behavioral Neuroscience* (in review)
- Ermentrout GB, Kopell N (1998) Fine structure of neural spiking and synchronization in the presence of conduction delays. *Proc Nat Acad Sci USA* 95:1259–1264
- Fishwick PA, Narayanan NH, Sticklen J, Bonarini A (1994) A multimodel approach to reasoning and simulation. *IEEE Transactions on Systems, Man, and Cybernetics* 24(10):1433–1449
- Fitzhugh R (1961) Impulses and physiological states in models of nerve membrane. *Biophysical Journal* 1:445–466
- Hairer E, Nørsett SP, Wanner G (1993) *Solving ordinary differential equations*, Volume 1. Springer
- Hodgkin AL, Huxley AF (1952) Currents carried by sodium and potassium ions through the membrane of the giant axon of *Loligo*. *Journal of Physiology* 117:500–544
- Hunter JD (2007) Matplotlib: A 2d graphics environment. *Computing in Science & Engineering* 9(3):90–95, DOI 10.1109/MCSE.2007.55, URL <http://dx.doi.org/10.1109/MCSE.2007.55>
- Jones C (1994) Geometric singular perturbation theory. In: Arnold L (ed) *Dynamical systems*, Montecatini Terme, Lecture notes in mathematics, vol 1609, Springer-Verlag, Berlin, pp 44–118
- Jones E, Oliphant T, Peterson P, et al (2001) SciPy: Open source scientific tools for Python. URL <http://www.scipy.org/>
- de Jong H, van Raalte F (1999) Comparative environment construction: A technique for the comparative analysis of dynamical systems. *Artificial Intelligence* 115:145–214
- Kopell N, Ermentrout GB, Whittington MA, Traub RD (1999) Gamma rhythms and beta rhythms have different synchronization properties. *Proc Natl Acad Sci USA* 97:1867–1872
- Lind D, Marcus B (1995) *An introduction to symbolic dynamics and coding*. Cambridge University Press
- Morris C, LeCar H (1981) Voltage oscillations in the barnacle giant muscle fiber. *Biophysical Journal* 35:193–213
- Oliphant TE (2006) *Guide to NumPy*. Provo, UT, URL <http://www.tramy.us/>
- Olyper AV, Calabrese RL (2007) Using constraints on neuronal activity to reveal compensatory changes in neuronal parameters. *Journal of Neurophysiology* 98:3749–3758
- Prinz AA, Bucher D, Marder E (2004) Similar network activity from disparate circuit parameters. *Nature Neuroscience* 7(12):1345–1353
- Reynolds D, Carlson JM, Doyle J (2002) Design degrees of freedom and mechanisms for complexity. *Phys Rev E* 66(016108)
- Rinzel J, Ermentrout GB (1989) Analysis of neural excitability and oscillations. In: Koch C, Segev I (eds) *Methods in Neuronal Modelling: From Synapses to Networks*, MIT Press, Cambridge, MA
- Rubin J, Wechselberger M (2007) Giant squid - hidden canard: the 3D geometry of the Hodgkin-Huxley model. *Biological Cybernetics* 97:5–32
- van der Schaft A (2004) Equivalence of hybrid dynamical systems. In: *Proc. of Mathematical Theory of Networks and Systems (MTNS 04)*
- van der Schaft AJ, Schumacher JM (2001) Compositionality issues in discrete, continuous, and hybrid systems. *International Journal of Robust and Nonlinear Control* 11:417–434
- Smolinski TG, Rabbah P, no CST, Nadim F, Prinz AA (2006) Analysis of biological neurons via modeling and rule mining. *International Journal of Information Technology & Intelligent Computing* 1(2):293–302
- Strogatz SH (2001) *Nonlinear Dynamics and Chaos*. Perseus Books
- Suckley R, Biktashev V (2003) The asymptotic structure of the Hodgkin-Huxley equations. *Int J Bifurcation & Chaos* 13(12):3805–3826
- Tien JH, Guckenheimer J (2008) Parameter estimation for bursting neuron models. *Journal of Computational Neuroscience* 24(3):358–373
- Villoslada P, Steinman L, Baranzini S (2009) Systems biology and its application to the understanding of neurological diseases. *Annals of Neurology* 65(2):124–139
- Wang XJ, Buzsáki G (1996) Gamma oscillation by synaptic inhibition in a hippocampal interneuronal network model. *Journal of Neuroscience* 16:6402–6413
- Zhao F (1994) Intelligent computing about complex dynamical systems. *Mathematics and Computers in Simulation* 36:423–432

A Model kinetics and parameters

For all three test models, the total ionic current is $\sum I_{\text{ionic}} = g_{Na} m h^3 (V - E_{Na}) + g_K n^4 (V - E_K) + g_L (V - E_L)$. For the Wang-Buzsáki model, $m = m_{\infty}(V)$, otherwise all gating variables are given by Eq. (2). The channel rate kinetics of any gating variable s are converted into s_{∞} and τ_s according to the standard definitions, $s_{\infty} = \alpha_s / (\alpha_s + \beta_s)$ and $\tau_s = 1 / (\alpha_s + \beta_s)$, for the forward and backward rate functions α_s and β_s , respectively.

A.1 Classic Hodgkin-Huxley model

$$\alpha_m = 0.1(V + 40)/(1 - \exp(-(V + 40)/10))$$

$$\beta_m = 4 \exp(-(V + 65)/18)$$

$$\alpha_h = 0.07 \exp(-(V + 65)/20)$$

$$\beta_h = 1/(1 + \exp(-(V + 35)/10))$$

$$\alpha_n = 0.01(V + 55)/(1 - \exp(-(V + 55)/10))$$

$$\beta_n = 0.125 \exp(-(V + 65)/80)$$

Parameter values: $g_{Na} = 120, g_K = 36, g_L = 0.3, E_{Na} = 50, E_K = -77, E_L = -54.4, I_{\text{applied}} = 8, C = 1$.

A.2 Wang-Buzsáki interneuron model

$$\alpha_m = 0.1(V + 35)/(1 - \exp(-(V + 35)/10))$$

$$\beta_m = 4 \exp(-(V + 60)/18)$$

$$\alpha_h = 0.35 \exp(-(V + 58)/20)$$

$$\beta_h = 5/(1 + \exp(-(V + 28)/10))$$

$$\alpha_n = 0.05(V + 34)/(1 - \exp(-(V + 34)/10))$$

$$\beta_n = 0.625 \exp(-(V + 44)/80)$$

Parameter values: $g_{Na} = 35, g_K = 9, g_L = 0.1, E_{Na} = 55, E_K = -90, E_L = -65, I_{\text{applied}} = 2.5, C = 1$.

A.3 Alternative interneuron model

$$\alpha_m = 0.32(V + 54)/(1 - \exp(-(V + 54)/4))$$

$$\beta_m = 0.28(V + 27)/(\exp((V + 27)/5) - 1)$$

$$\alpha_h = 0.128 \exp(-(50 + V)/18)$$

$$\beta_h = 4/(1 + \exp(-(V + 27)/5))$$

$$\alpha_n = 0.032(V + 52)/(1 - \exp(-(V + 52)/5))$$

$$\beta_n = 0.5 \exp(-(57 + V)/40)$$

Parameter values: $g_{Na} = 100, g_K = 80, g_L = 0.1, E_{Na} = 100, E_K = -100, E_L = -67, I_{\text{applied}} = 2, C = 1$.

A.4 Leech heart interneuron

The details of the channel kinetics are given in Cymbalyuk et al (2002). All channels are given by the standard Hodgkin-Huxley formalism. The parameters for the tonic spiking regime of the HN interneuron model were: $g_L = 8.0, E_L = -60, g_{CaF} = 5, g_{CaS} = 3.2, E_{Ca} = 135, g_{K1} = 100, g_{K2} = 80, g_{KA} = 80, E_K = -70, g_H = 4, E_H = -21, g_P = 7, E_{Na} = 45, g_{Na} = 200, I_{\text{applied}} = 0, C = 0.5$.

B Dominant scale sets for the original neuron models

The \mathcal{A}_Ψ and \mathcal{A}_Ω sets for the periodic orbit of the Type II Hodgkin-Huxley model are shown in Tables 2 and 3, using $\sigma = \gamma = 4$. The time intervals for each epoch are not contiguous due to the discrete time points from the numerically computed periodic orbit. However, the dominant scales method does not require the transitions to be computed more accurately. A graphic view of these transitions overlaid on the periodic orbit is presented in Fig. 2. Corresponding sets for the Type I HH and Wang-Buzsáki models are shown in Tables 4–7. In these tables, variables are labeled fast or slow only if they belong to \mathcal{F} or \mathcal{S} for the entire epoch. All times are shown to the nearest 1/100 ms.

Table 2 Ordered sets of active and modulatory variables during one period of the Type II HH model orbit, using Ψ . x^S denotes $x \in \mathcal{S}$.

#	Time interval	\mathcal{A}_Ψ	\mathcal{M}_Ψ
1	[0.00, 5.16]	n^S	m, a, l
2	[5.26, 9.16]	n^S, m	a, h^S, l
3	[9.26, 12.86]	m, n^S	h^S, a
4	[12.96, 13.04]	m, n^S, h^S	l, a
5	[13.10, 13.30]	n^S, m, h^S	l, a
6	[13.34, 13.57]	n^S, h^S, m	l, a
7	[13.61, 13.77]	n^S, h^S, m^S	l, a
8	[13.80, 15.25]	h^S, n^S, m^S	l, a
9	[15.31, 15.49]	h^S, m, n^S	a, l
10	[15.55, 15.61]	m, n^S, h^S	a, l
11	[15.66, 15.71]	n^S, m	h^S, a, l
12	[15.78, 15.97]	n^S	m, a, l

Table 3 Ordered sets of active and modulatory variables during one period of the Type II HH model orbit, using Ω . x^S denotes $x \in \mathcal{S}$.

#	Time interval	\mathcal{A}_Ω	\mathcal{M}_Ω
1	[0.00, 6.06]	n^S	m, h^S
2	[6.16, 7.26]	n^S, m	h^S
3	[7.36, 8.06]	m, n^S	h^S
4	[8.16, 9.46]	m	n^S, h^S
5	[9.56, 11.86]	m, n^S	h^S
6	[11.96, 13.15]	m	n^S, h^S
7	[13.22, 13.34]	m, n^S	h^S
8	[13.37, 13.42]	m, n^S, h^S	
9	[13.45, 13.52]	n^S, m, h^S	
10	[13.57, 13.65]	n^S, h^S, m	
11	[13.68, 13.94]	n^S, h^S	m^S
12	[13.96, 14.25]	h^S, n^S	m^S
13	[14.28, 14.38]	h^S, n^S, m^S	
14	[14.41, 14.57]	h^S, m^S, n^S	
15	[14.62, 14.84]	m^S, h^S	n^S
16	[14.89, 15.25]	m^S	h^S, n^S
17	[15.31, 15.66]	m	h^S, n^S
18	[15.71, 15.78]	m, n^S	h^S
19	[15.88, 15.97]	n^S	m

Table 4 Ordered sets of active and modulatory variables during one period of the Type I HH model orbit, using Ψ . x^S denotes $x \in \mathcal{S}$, x^F denotes $x \in \mathcal{F}$.

#	Time interval	\mathcal{A}_Ψ	\mathcal{M}_Ψ
1	[0.00, 0.35]	n	l, a
2	[0.45, 1.15]	n^F	a, l
3	[1.25, 1.55]	n^F, a, l	m^F
4	[1.65, 1.95]	a, l, n^F	m^F
5	[2.05, 4.15]	a, l	n^F, m^F
6	[4.25, 6.75]	l, a	m^F
7	[6.85, 8.05]	l, a, m^F	n^F
8	[8.15, 9.65]	m^F, l, a	n^F
9	[9.75, 9.85]	m^F, l	l, a
10	[9.95, 13.65]	m^F	n, l, a
11	[13.75, 13.94]	m^F, n	l, h
12	[13.97, 13.99]	m, n	h^S, l
13	[14.01, 14.19]	n^S, m	h, l
14	[14.20, 14.28]	n^S, m, h^S	l
15	[14.29, 14.45]	n^S, h^S, m	l, a
16	[14.47, 14.63]	h^S, n^S, m	a, l
17	[14.66, 14.68]	m, n^S, h^S	l, a
18	[14.70, 14.73]	m, n^S, h^S	l, a
19	[14.75, 14.77]	m, n^S	h^S, l, a
20	[14.81, 14.86]	n^S, m	m, l, a
21	[14.90, 15.10]	n	l, a

Table 5 Ordered sets of active and modulatory variables during one period of the Type I HH model orbit, using Ω . x^S denotes $x \in \mathcal{S}$, x^F denotes $x \in \mathcal{F}$.

#	Time interval	\mathcal{A}_Ω	\mathcal{M}_Ω
1	[0.00, 0.35]	n	m^F, h
2	[0.45, 3.85]	n^F	m^F
3	[3.95, 4.05]	n^F, m^F	h^F
4	[4.15, 4.35]	m^F, n^F	h^F
5	[4.45, 13.94]	m^F	n
6	[13.97, 14.08]	m	n
7	[14.02, 14.07]	m, n^S	h
8	[14.08, 14.12]	n^S, m	h^S
9	[14.13, 14.17]	n^S	h^S, m
10	[14.19, 14.35]	n^S, h^S	m
11	[14.36, 14.43]	h^S, n^S	m
12	[14.45, 14.47]	h^S, m, n^S	
13	[14.49, 14.54]	m, h^S	h^S, n^S
14	[14.55, 14.75]	m	n^S, h^S
15	[14.77, 14.81]	m, n^S	h^S
16	[14.86, 15.10]	n	m

Table 6 Ordered sets of active and modulatory variables during one period of the Type I WB model orbit, using Ψ . x^S denotes $x \in \mathcal{S}$, x^F denotes $x \in \mathcal{F}$.

#	Time interval	\mathcal{A}_Ψ	\mathcal{M}_Ψ
1	[0.00, 0.58]	n^F	m^F, a, l
2	[0.68, 0.98]	n^F, m^F	a, l
3	[1.08, 1.28]	n^F, m^F, a, l	h^F
4	[1.38, 1.78]	m^F, n^F, a, l	h^F
5	[1.88, 2.38]	m^F, n^F	l, a
6	[2.48, 6.08]	m^F	n^F, l, a, h
7	[6.18, 6.34]	m^F, n	h, l
8	[6.39, 6.49]	m^F, n, h	l
9	[6.50, 6.52]	n, m^F, h	l
10	[6.53, 6.54]	n^S, m^F, h	l
11	[6.56, 6.57]	n^S, h, m^F	l
12	[6.59, 6.71]	n, h, m^F	l
13	[6.74, 6.80]	h, n, m^F	l, a
14	[6.84, 6.90]	h, n	m^F
15	[6.95, 7.22]	h	n, m^F
16	[7.28, 7.34]	h, n, m^F	a, l
17	[7.41, 7.46]	n, m^F, h	h, a, l
18	[7.55, 8.35]	n	m^F, a, l

Table 7 Ordered sets of active and modulatory variables during one period of the Type I WB model orbit, using Ω . x^S denotes $x \in \mathcal{S}$, x^F denotes $x \in \mathcal{F}$.

#	Time interval	\mathcal{A}_Ω	\mathcal{M}_Ω
1	[0.00, 1.28]	n^F	m^F, h
2	[1.38, 1.68]	n^F, m^F	h^F
3	[1.78, 2.18]	m^F, n^F	h^F
4	[2.28, 6.53]	m^F	h, n
5	[6.54, 6.56]	m^F, n^S, h	-
6	[6.57, 6.59]	n, h, m^F	m^F
7	[6.60, 6.84]	n, h	m^F
8	[6.90, 6.95]	h, n	m^F
9	[7.05, 7.12]	m^F, h	h, n
10	[7.18, 7.34]	m^F	n, h
11	[7.41, 7.46]	m^F, n	h
12	[7.55, 8.35]	n	m^F, h